UC Santa Cruz
UC Santa Cruz Previously Published Works

Title
Geometric influence on the net magnetic moment in LaCoO3 thin films

Permalink
https://escholarship.org/uc/item/7j55f29r

Journal
Journal of Materials Research, 38(8)

ISSN
0884-2914

Authors
Joshi, T
Belanger, DP
Tan, YT
et al.

Publication Date
2023-04-28

DOI
10.1557/s43578-023-00957-3

Copyright Information
This work is made available under the terms of a Creative Commons Attribution License, availalbe at https://creativecommons.org/licenses/by/4.0/

Peer reviewed

Geometric influence on the net magnetic moment in LaCoO₃ thin films

T. Joshi[1], D. P. Belanger[1,a)] (ID), Y. T. Tan[2], W. Wen[3], D. Lederman[1]

[1] *Department of Physics, University of California, Santa Cruz, CA 95064, USA*
[2] *Sibley School of Mechanical and Aerospace Engineering, Cornell University, Ithaca, NY 14853, USA*
[3] *Shanghai Institute of Applied Physics, Chinese Academy of Sciences, Pudong New District, Shanghai 201204, China*
a) Address all correspondence to this author. e-mail: daveph@ucsc.edu

The different magnetic behaviors of LaCoO₃ films grown on LaAlO₃ and SrTiO₃ substrates are related to the Co–O–Co bond angles and the constraints imposed on the Co–O bond lengths by the substrate geometries. The observed magnetic behavior is not consistent with ferromagnetism. Rather, long-range antiferromagnetic order occurs below $T \approx 90$ K when the Co–O–Co bond angle is greater than 163°, consistent with the behavior of bulk and nanoparticles forms of LaCoO₃. A LaAlO₃ substrate prevents magnetic long-range order at low temperatures near the film–substrate interface and collinear antiferromagnetic sublattices away from the interface. At low temperatures, the antiferromagnetically ordered sublattices are non-collinear in films grown on SrTiO₃ substrates, leading to a significant net moment. The net moment is controlled by the geometry imposed by the substrate upon which the LaCO₃ film is grown.

Introduction

LaCoO₃ (LCO) in bulk crystalline form exhibits a small net moment below a temperature of $T \approx 89$ K. The moment arises from an asymmetry of the antiferromagnetic sublattices induced by the structural geometry at twin plane interfaces along (100) pseudocubic planes of the lattice [1]. Away from the twin boundaries, for temperatures above 100 K, fits to Curie–Weiss behavior indicate antiferromagnetic interactions [2], with $\theta_{CW} \approx -182(4)$ K, between atomic moments of 3.45(2) μ_B, yet bulk LCO does not order antiferromagnetically at low temperatures because the thermally activated interactions are reduced as T decreases before the transition can take place. The strength of the magnetic interactions has been correlated with the angle of tilt between adjacent oxygen octahedra surrounding Co ions, given by the Co–O–Co bond angle. As the temperature decreases toward $T = 40$ K, the average magnetic interaction weakens as the Co–O–Co angle decreases toward a critical angle of 163° [2–5]. The critical angle of 163° found experimentally is consistent with results from generalized gradient approximation calculations [6]. When the temperature is below $T = 40$ K, the angle no longer changes and the interaction strength is insufficient to support ordering. The magnetic state

is thermally activated above $T = 40$ K [3, 6]. This mechanism does not rely on proposed [7] thermally excited intermediate spin-state ($t_{2g}^5 e_g^1$) transitions that could become possible with Jahn–Teller-like distortions of Co–O bonds in the oxygen octahedra; neutron scattering and extended x-ray absorption fine structure (EXAFS) studies found no significant evidence of the necessary distortion of the octahedra in bulk or nanoparticle forms of LCO [8, 9].

The correlation between the behavior of antiferromagnetism and the Co–O–Co angle applies consistently for bulk and nanoparticle forms of LCO [1–5], but the magnetization of thin-film samples has not previously been examined in that context. Here we show evidence that this correlation does hold in films, even though the film geometries are distorted by the strain from the substrates upon which they are grown. We also show evidence that the behaviors of LCO thin films grown on SrTiO₃ (STO) and on LaAlO₃ (LAO) are consistent with antiferromagnetism, but not ferromagnetism. The geometric influences of the substrates give a common basis for understanding why strikingly different magnetic behaviors appear under different strain conditions and why they can be influenced in the case of SrTiO₃ substrates [10].

A large number of studies have addressed the magnetic behavior of LCO films on STO and LAO substrates [11–28]. A common assumption for many studies of LCO films on STO substrates, in which a net spontaneous moment occurs, has been that the interactions in the film are ferromagnetic. Likewise, it has often been stated that LCO films on LAO substrates are paramagnetic. No model has been developed that adequately explains why ferromagnetic interactions would appear in LCO films on STO substrates, but not on LAO substrates and not in bulk or nanoparticle forms of LCO. One of the striking characteristics of LCO films, as well as bulk and nanoparticle forms of LCO, is that long-range order, if present, tends to occur within the temperature range of $65 < T < 90$ K. This suggests a common interaction, likely antiferromagnetic as they are in other forms of LCO, regardless of whether a net moment appears. Here we show, using magnetometry and structural data, that the films behave in ways consistent with bulk LCO in that the interactions are antiferromagnetic, but only when the Co–O–Co bond angles are greater than approximately 163°. We also show that their behavior is not consistent with ferromagnetic interactions. Instead, the STO substrates strain the LCO films in a way that induces a net moment via antiferromagnetic sublattices that are non-collinear. In contrast, close to the interfaces of LCO films with LAO substrates, magnetic interactions for bonds in planes parallel to the interfaces are suppressed and no magnetic long-range order takes place at low temperatures. Further from the LCO/LAO interface, the LCO lattice relaxes toward the bulk LCO structure and this allows ordering with antiferromagnetic collinear sublattices, resulting in no net moment. In the geometric interpretation, it is the substrate strain that controls the appearance of the net moment in LCO films through non-collinear alignment of antiferromagnetic sublattices, not the appearance of ferromagnetic interactions. Switching between a state with no net magnetic moment to one that has a significant net moment, as has been observed in devices [10], is controlled by the nature and size of the strain imposed by the substrate. This geometric interpretation correlating the Co–O–Co angle to the appearance of a net moment is based on data obtained from x-ray scattering and magnetometry measurements of thin LCO films.

Results and discussion

Sample structure

X-ray diffraction and synchrotron spectra for a 25.7-nm-thick LCO film on STO and a 26-nm-thick film on LAO are shown in Fig. 1(a) and (b), respectively. The synchrotron data are of higher resolution and show interference peaks clearly. The shift in the Bragg peak position of the films relative to bulk LCO (vertical solid line) corresponds to a change in c lattice parameter
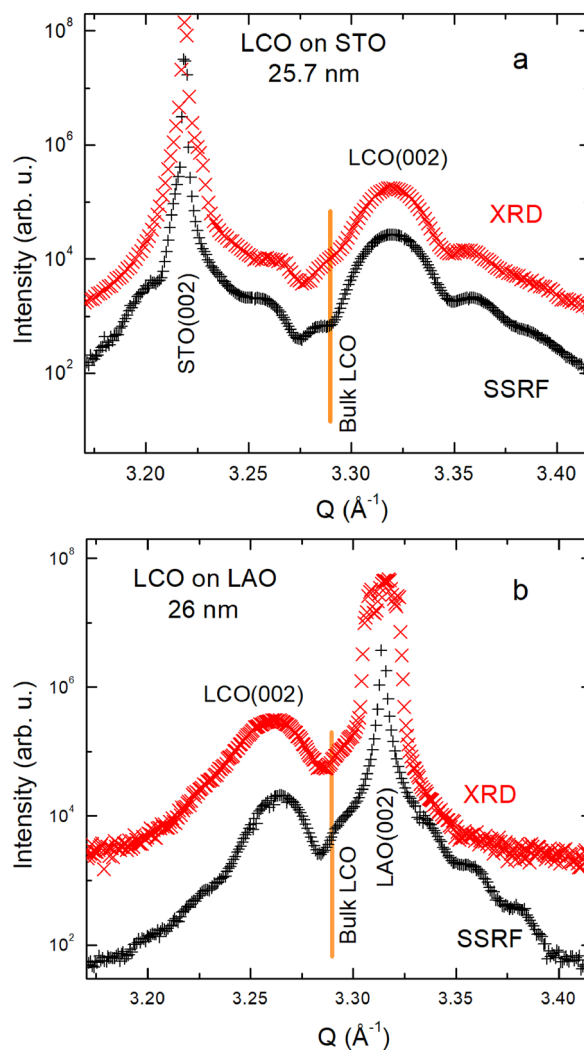
Figure 1: X-ray diffraction (XRD) and high-resolution synchrotron spectra (SSRF) for a 25.7-nm-thick LCO film on STO (001) (a) and a 26-nm-thick film on LAO (001) (b). The orange solid lines represent the bulk peak position.

originating from the tensile strain on the LCO film parallel to the substrate induced by STO and compression parallel to the substrate induced by LAO. X-ray diffraction spectra for three of the films with different film thicknesses grown on STO substrates are shown in Fig. 2(a) and Fig. S1 (Supplementary Material). The spectra show a progressive shift in the LCO (003) peak position toward the left side of the figure due to the partial lattice relaxation with increased film thickness. The 25.7-nm film shows a split in the peak corresponding to the relaxed and strained portions of the film. The reciprocal space map of the (103) reflection indicated that the film was lattice matched with the substrate (see Fig. S2 in the Supplementary Material). AFM images of LCO films on STO are shown in Fig. S3 (Supplementary Material). For thinner films the atomically smooth terraces of the substrate were evident on the film surface, but as the films
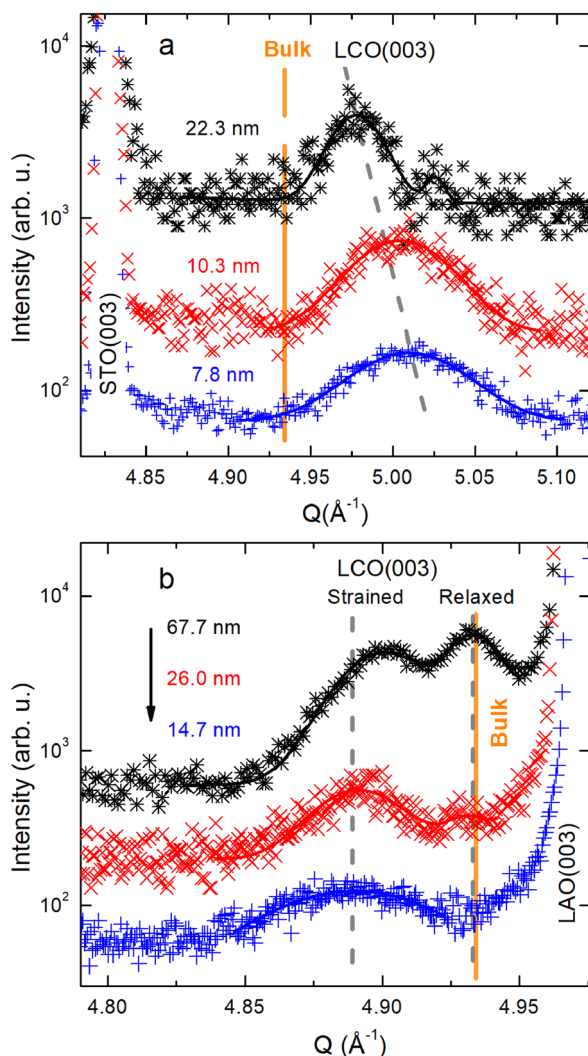
Figure 2: (a) X-ray diffraction spectra measured for LCO films on STO substrates. The gray-dashed line is a visual guide for the shift in the film peak position with increasing film thickness. The shift corresponds to the different strain states in the film. (b) X-ray diffraction spectra measured from LCO films grown on LAO substrates. The two dashed lines indicate the peak positions of the strained (left) and relaxed part of the film in thicker films. The solid curves are Gaussian fits to the LCO peaks.

TABLE 1: LCO films on LAO and STO substrates including film thicknesses determined from x-ray reflectivity (t_{XRR}) and synchrotron x-ray diffraction (t_{SSRF}) and room-temperature c and a lattice parameters.

Substrate	t_{XRR} (nm)	t_{SSRF} (nm)	c (Å)	a (Å)	c/a
LAO	11.5 (2)	–	3.877 (8)	3.791	1.023 (2)
LAO	14.7 (3)	10.4 (28)	3.865 (6)	3.791	1.022 (2)
LAO	26.0 (2)	23.0 (20)	3.868 (7)	3.791	1.020 (2)
LAO	67.5 (4)	–	3.846 (4)	3.791	1.015 (1)
LAO	67.5 (4)*	–	3.818 (5)	–	–
STO	7.8 (3)	6.0 (3)	3.763 (8)	3.905	0.964 (1)
STO	10.3 (5)	–	3.773 (5)	3.905	0.966 (1)
STO	22.3 (3)	–	3.787 (1)	3.905	0.970 (1)
STO	25.7 (2)	19.1 (16)	3.786 (3)	3.905	0.970 (1)
LAO	40.7 (10)**	–	3.789 (9)	–	–

*Second peak of 67.5-nm film.

**LCO/STO multilayer film.

The values of a correspond to the in-plane lattice constants of the substrate. Uncertainties of the last digit are in parentheses.

the crystalline coherence length, whereas the reflectivity is not sensitive to the crystallinity, but rather only to surface and interface roughness. It is worth noting that the beam used at the synchrotron consists of a spot approximately 500 μm in diameter, which is smaller than the $\approx 5 \times 1\,\text{mm}^2$ beam used in the traditional x-ray diffractometer, and this is why the fringes are better defined in the synchrotron measurements.

The room-temperature c and a lattice parameters of all of the LCO films on LAO and STO substrates are also listed in Table 1. The c lattice parameters are calculated using x-ray Bragg diffraction peaks. The values for the a lattice parameters shown are the well-known values of the substrates. The assumption that the in-plane lattice constants conform to the substrate may not be true for the entire thickness of the 26.0- and 67.7-nm films on LAO due to the presence of the relaxed phase peak in Fig. 2; in those two cases, the upper portion of the film relaxes at a critical thickness greater than 14.7 nm to the bulk lattice constant. It is the pseudo-relaxed portion of the film which is responsible for the antiferromagnetic behavior; the small amount of strain remaining is enough to create a bond angle greater than the critical value of 163°. The truly bulk behavior is approached probably exponentially with thickness, so it might take a film thicker than 100 nm, or perhaps 500 nm, to achieve the fully collinear antiferromagnetic arrangement of bulk LCO.

Temperature dependence

As a result of the small volume of the LCO film relative to that of the substrate, the significant diamagnetic contribution present in the magnetometry data of the combined film and substrate must be carefully accounted for in the analysis of the LCO film magnetic behavior. To accomplish this, after measurements on

became thicker, the surface roughness increased and topography became more granular. Films grown on LAO, which have a relatively smaller film–substrate lattice mismatch, on the other hand, showed a smaller peak shift with increased film thickness [Fig. 2(b)]. Peak splitting for the thicker films was observed due to the lattice relaxation, similarly to the film grown on STO.

The thickness of the films calculated from x-ray reflectivity (Fig. S4, Supplementary Material) and synchrotron spectra is listed in Table 1. The thickness values calculated from synchrotron data (using the Laue fringes visible around the Bragg peak) are consistently smaller than those calculated from x-ray reflectivity because the x-ray diffraction data are sensitive to

an LCO film on the substrate, the film was etched off chemically by dipping the sample into aqua regia, as discussed in the Method section, and the magnetic measurements were repeated on the substrate with both field orientations and identical measurement conditions.

To analyze the magnetic behavior of the films over the wide temperature range $5 < T < 320$ K, it works well to subtract the magnetic substrate signal by simply subtracting the substrate magnetic data directly. To analyze the LCO film magnetism on STO substrates well above the transition, where the signal is relatively weak, we used the fits to the substrate data and subtracted them from the data taken with the films on the substrates. For 22.3- and 25.7-nm films on STO, data taken under conditions of high thermal stability fit well to a Curie-like dependence plus a constant, given by

$$\frac{M}{H} = \frac{C}{(T - \Theta_{CW})} + B,$$ (1)

over the range $90 < T < 320$ K, where C is a constant, Θ_{CW} is the Curie–Weiss temperature, and B is a constant background. The fits for the substrate-only data were carried out with $\Theta_{CW} = 0$. Using these fits to analyze the film magnetism over this temperature range yielded essentially the same results as when the substrate were directly subtracted from the substrate data, but using the fits resulted in slightly less noise and a smaller residual background. For LCO films on LAO, even with high thermal stability, we simply subtracted the substrate data directly over this range because we could not obtain fits to a critical behavior as a function of T for $T < T_N$ given by

$$M = A(T_N - T)^\beta + B,,$$ (2)

where T_N is the critical transition temperature and B is a constant background, without adding at least one additional fitting parameter, such as a linear term proportional to T. However, doing so resulted in error estimates for T_N and B that were so large that the fits were deemed not to be meaningful.

The magnetic behavior of the 67.5-nm film, after subtracting the signal from the LAO substrate, is shown in Fig. 3(a) for $5 < T < 320$ K and $\mu_0 H = 100$ mT, with the field applied in the plane of the substrate and perpendicular to it. For this sample, particular attention was paid to the thermal stability while taking data in order to characterize the small signal for $T > 100$ K using Eq. 1, but no credible fits were possible. The magnetization is weak and the Curie–Weiss temperature is negative, so the signal has little variation with temperature over the fitting range; the Curie–Weiss temperature is highly correlated with the constant background in the fits, leading to very large parameter uncertainties. Below $T \approx 100$ K, a small moment appears which is approximately twice as large in the in-plane measurements. The data do not follow critical behavior expected for an order parameter conjugate to the applied field close to the transition
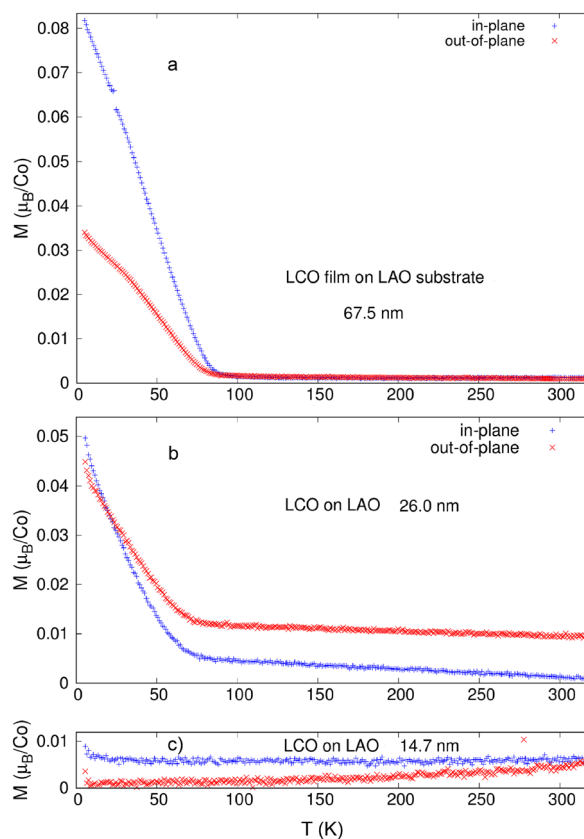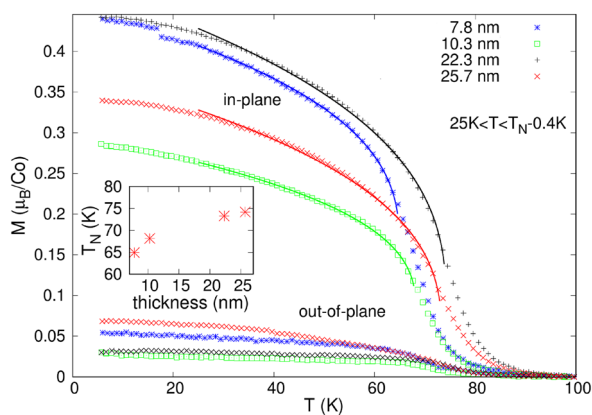

Figure 3: Magnetization M as a function of temperature T for films grown on LAO in an external field $\mu_0 H = 100$ mT after subtracting the signal from the substrate. The films were (a) 67.5 nm, (b) 26.0 nm, and (c) 14.7 nm thick.

temperature T_N given by Eq. 2, but rather indicate a spin-flop-like signal associated with antiferromagnetic ordering below $T_N \approx 90$ K. Such behavior is to be expected for antiferromagnetic order in small applied fields when there is small or negative uniaxial or cubic anisotropy [1]. In contrast to bulk LCO, however, the LCO film magnetic interactions extend to low temperatures. We conclude that the moments form two sublattices that order collinearly. The transition temperature is consistent with the size of the magnetic moments and the interaction strength found in bulk LCO at temperatures between 150 K and room temperature and at all temperatures below room temperature in LCO nanoparticles [1–5].

Figure 3 demonstrates the effect of reducing the film thickness. For a 26-nm-thick film [Fig. 3(b)], the spin-flop-like signal is still apparent, but the magnetic signal per Co ion is reduced relative to the 67.5-nm film. With a further reduction to a thickness of 14.7 nm [Fig. 3(c)], there is no evidence of spin-flop ordering. Although the thermal stability was not as high, so the substrate background data are not as accurately subtracted as for the 67.5-nm sample, the decrease in ordering with thinner films is apparent.

The behavior of LCO films on STO substrates contrasts that of LCO films on LAO substrates. Figure 4 shows data from four LCO films with thicknesses 7.8, 10.3, 22.3, and 25.7 nm with the field in the plane of the film and perpendicular to it. As discussed above, the significant non-magnetic background must be subtracted over the $5 < T < 100$ K temperature range shown in the figure. We first compensated for most of the background by subtracting the substrate data directly from the film plus substrate data. Because this left a small background that varied from sample to sample, the data were shifted vertically to ensure they passed through zero at $T = 100$ K, so the resulting plots mostly represent the magnetic ordering. The measured magnetization perpendicular to the films is much smaller than in the plane and could simply be a result of imperfect alignment of the film with the film with the field or slight amount of film disorder. A small sample-to-sample variation in the magnetization, on the other hand, is probably due to the shape anisotropy field of the thin-film geometry as discussed in Ref. [29].

For the in-plane signal, M vs. T is shown in Fig. 4 along with fits to Eq. 2. The order parameter critical exponent was fixed to the three-dimensional Heisenberg value of $\beta = 0.37$ and the other parameters were allowed to vary. The values of T_N obtained from the fits are shown in the inset. The amplitudes vary somewhat. It has recently been shown that there can be effects at low temperature from crystal twins [13], but not near the transition temperature; the critical amplitudes might be more affected by slight disorder and initial cooling rates. The fits are reasonable, despite being done for temperatures $25 < T < T_N - 0.4$ K which include data 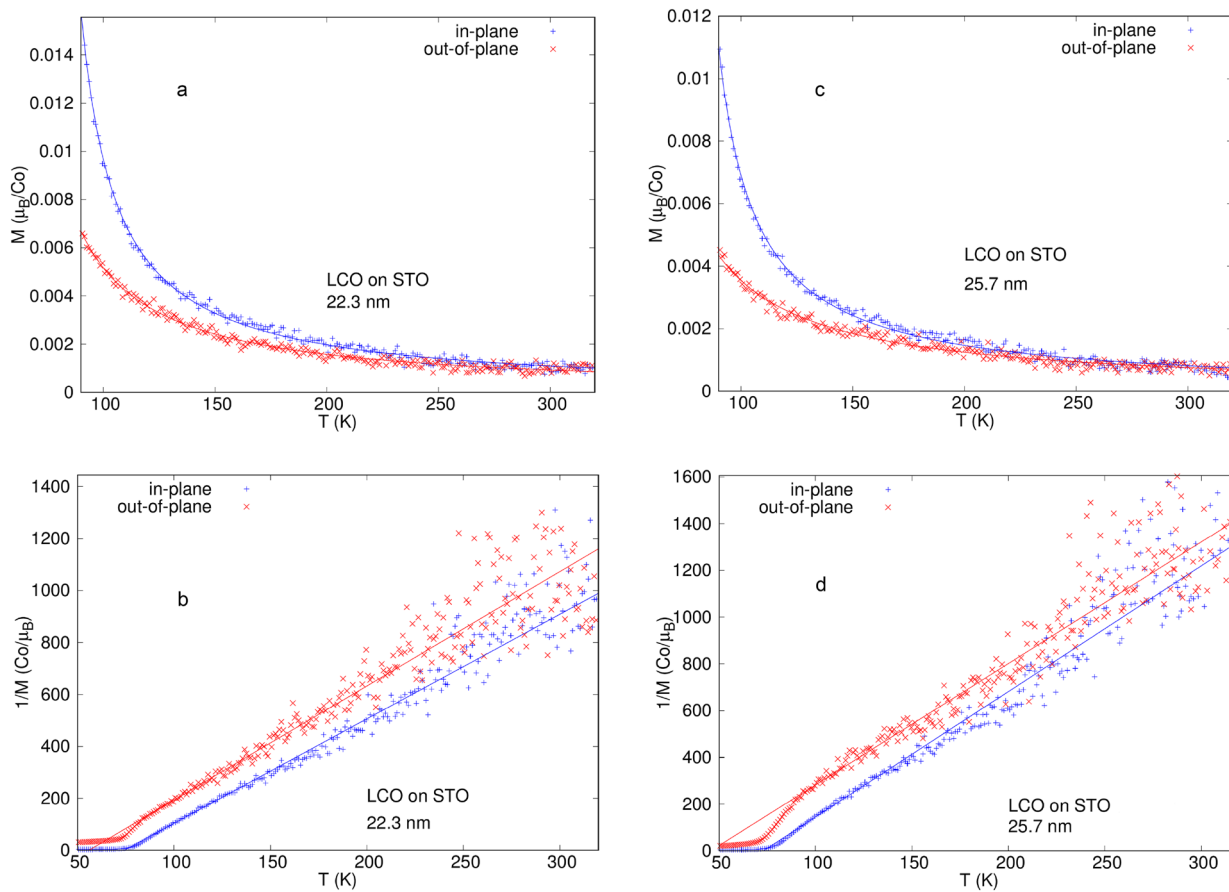likely well outside the asymptotic critical region. The compatibility with the three-dimensional Heisenberg critical exponent sharply contrasts the behavior found for bulk LCO, where $\beta \approx 0.7$ resulting from surface ordering at twin interfaces [1, 5, 30, 31].

For temperatures above $T = 100$ K, the magnetic signal is too weak in the 10.3- and 7.8-nm films to allow reliable fits, but good fits were obtained for the 22.3- and 25.7-nm films. Excellent fits to Eq. 1 between $T = 120$ and 320 K were obtained for the two LCO films on STO after subtracting fits to the substrate data, as shown in Fig. 5(a) and (c). The same results are shown as $1/M$ vs. T in Fig. 5(b) and (d) to illustrate the straight line behavior at higher temperatures and the consistent behavior of the two samples. Values for the effective moment per Co ion, μ_{eff}, in units of μ_B, the Bohr magneton, are calculated using

$$\mu_{\mathrm{eff}} = \left(\frac{3k_B C}{n\mu_0\mu_B^2} \right)^{1/2},\quad (3)$$

where k_B is the Boltzmann's constant and n is the number of Co atoms per unit volume. The parameters C and μ_{eff} obtained from the fits (Table 2) are fairly consistent for the two samples and the two field orientations, and the values for μ_{eff} are close to the value $3.45(2)\mu_B$ obtained for bulk LCO [2]. The positive values of θ_{CW} are consistent with the ordering of a net moment; they do not necessarily indicate ferromagnetic interactions. In ferromagnetic materials, where the applied field is conjugate to the order, the Curie–Weiss parameter is positive and roughly reflects the net strength of the interactions and, thus, the transition temperature. The applied field normally does not couple directly to antiferromagnetic ordering and, consequently, the Curie–Weiss temperature is negative with a magnitude roughly corresponding to the transition temperature. However, when the magnetic moments in an antiferromagnetic materials are canted as a result of a structural distortion, the field does couple to the non-collinear antiferromagnetic ordering, and the Curie–Weiss temperature will exhibit a positive value with a magnitude reflecting the strength of the net antiferromagnetic interactions. Such is the case of a LCO thin film on a STO substrate. Good fits to the magnetization well above T_N are possible in this case because the positive values of θ_{CW} result in a significant variation with temperature in the fitting region.

To explore whether the interface chemistry plays a role in the nature of the ordering and to see the effect of imposed lattice constraints intermediate to those imposed by the LAO and STO substrates, the M vs. T data of an epitaxial multilayer consisting of a 13.9-nm STO capping layer, a 40-nm LCO layer, a 37.8-nm STO layer, and a 9.4-nm LCO buffer layer grown on a LAO substrate were measured with an external field $\mu_0 H = 100$ mT in the plane of the sample and perpendicular to it. Although LCO interfaces directly with STO, but not LAO, there is no evidence of ordering involving a net moment, as shown in Fig. 6. The Bragg peak of the LAO is
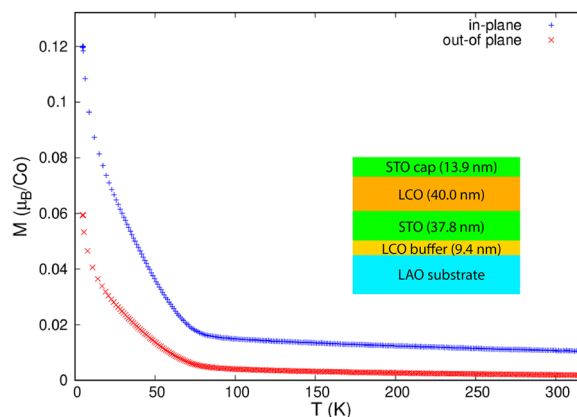

Figure 4: Magnetization M as a function of temperature T for four LCO films on STO substrates measured in a magnetic field of $\mu_0 H = 100$ mT. The upper data sets are for H in the plane of the film and the lower sets are for H perpendicular to the plane of the film. The data are adjusted vertically so that they pass through zero at $T = 100$ K. The curves are fitted to Eq. 2 over the range $25 < T < T_N - 0.4$ K, with β fixed to 3D Heisenberg value 0.37. The inset shows fitted values for T_N as a function of film thickness.

Figure 5: Magnetization *M* as a function of temperature *T* for the 22.3- and 25.7-nm-thick LCO films on STO substrates with an external field $\mu_0 H = 100$ mT applied in-plane and out-of-plane of the sample. (a) Film data fitted to Eq. 1 after subtracting a fit of the substrate data to Eq. 1 for the 22.3-nm film. (b) Inverse magnetization $1/M$ vs. *T* of the 22.3-nm film to illustrate the straight line behavior and positive Curie–Weiss temperature. Panels (c) and (d) are similar to panels (a) and (b) but correspond to the 25.7-nm-thick sample.

TABLE 2: LCO/STO fit parameters and moments using Eq. 1.

Thickness (nm)	Field orientation	*C* (K)	θ_{CW} (K)	μ_{eff} (μ_B)
22.3	In-plane	0.247 (3)	74 (1)	3.33 (2)
	Out of plane	0.23 (1)	56 (1)	3.18 (5)
25.7	In-plane	0.245 (4)	73 (1)	3.31 (3)
	Out of plane	0.25 (1)	46 (2)	3.37 (8)

Uncertainties in the last digit are in parenthesis.

broad with a full width at half maximum of 1.2° (Fig. S5, Supplementary Material), indicating a significant spread in *c*-axis lattice parameter values within the sample, but a fit to the peak position yields an average *c*-axis lattice parameter value intermediate between the cases of LCO interfacing directly with LAO and interfacing with STO, as shown in Table 1. It appears that the operating influence on the LCO film is not the chemistry of the interface, but rather the degree of strain distorting the LCO lattice. This is consistent with the voltage-controlled
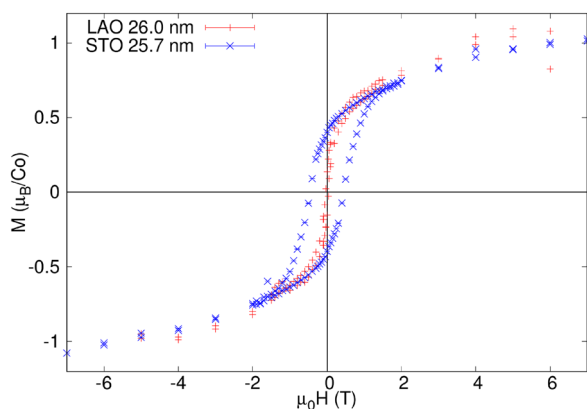

Figure 6: Magnetization *M* as a function of temperature *T* for a LCO/STO multilayer film with a top 13.9-nm STO layer, a 40.7-nm LCO layer, a 37.8-nm STO layer, and a 9.4-nm LCO layer on a LAO substrate with $\mu_0 H = 100$ mT after subtracting the non-magnetic background by fitting the data for *T* > 150 K to Eq. 1. As discussed in the text, the LAO substrate has a complex temperature dependence which is further complicated by the STO layers and the STO/LAO interactions. However, it is clear that antiferromagnetic ordering takes place without a net moment and is stronger than the LCO films on LAO substrates.

strain used to switch the net moment on and off in a LCO layer of a multilayer device [10].

Magnetic field dependence

The M vs. H behavior at $T = 5$ K for $\mu_0 H \leq 7$ T of two LCO films with thicknesses near 26 nm grown on a LAO substrate and 25.7-nm film grown on a STO substrate is compared in Fig. 7 after proper subtraction of background signals from the substrate. The film grown on LAO shows little hysteresis (small coercivity), consistent with ordering of collinear antiferromagnetic lattices. The film grown on STO shows hysteresis below $\mu_0 H = 2$ T, consistent with the observation of the net moment associated with canting of the antiferromagnetic ordering. The moments at higher fields are approximately the same for the two films. The moments at $\mu_0 H = 7$ T are significantly smaller than the moments indicated by the Curie–Weiss fits to LCO on STO substrates, but the moments do not saturate at this field.

The field-dependent behavior of M vs. T was investigated for $0.05 < \mu_0 H < 0.5$ T. The background was subtracted as described earlier. A ferromagnetic material should exhibit rounding of the transition with increasing field. No such rounding is observed in LCO on STO substrates; the transition remains sharp as seen in Fig. 8(a) which shows the magnetic ordering below T_N. The solid curves are fits to Eq. 2 using $\beta = 0.37$ for T between 30 K and T_N for four field values. The value $\beta = 0.37$ was chosen because the exchange interaction is not strongly anisotropic (the anisotropic value $\beta = 0.33$ is not significantly different), but the fits are not strongly sensitive to small changes in the value. The fits work well for the range of T fitted, but the data fall significantly below the fits for $T < 30$ K. The magnetic net moment has two distinct contributions. The first is from the canted components of the moments that reflect the antiferromagnetic order critical behavior. The second is
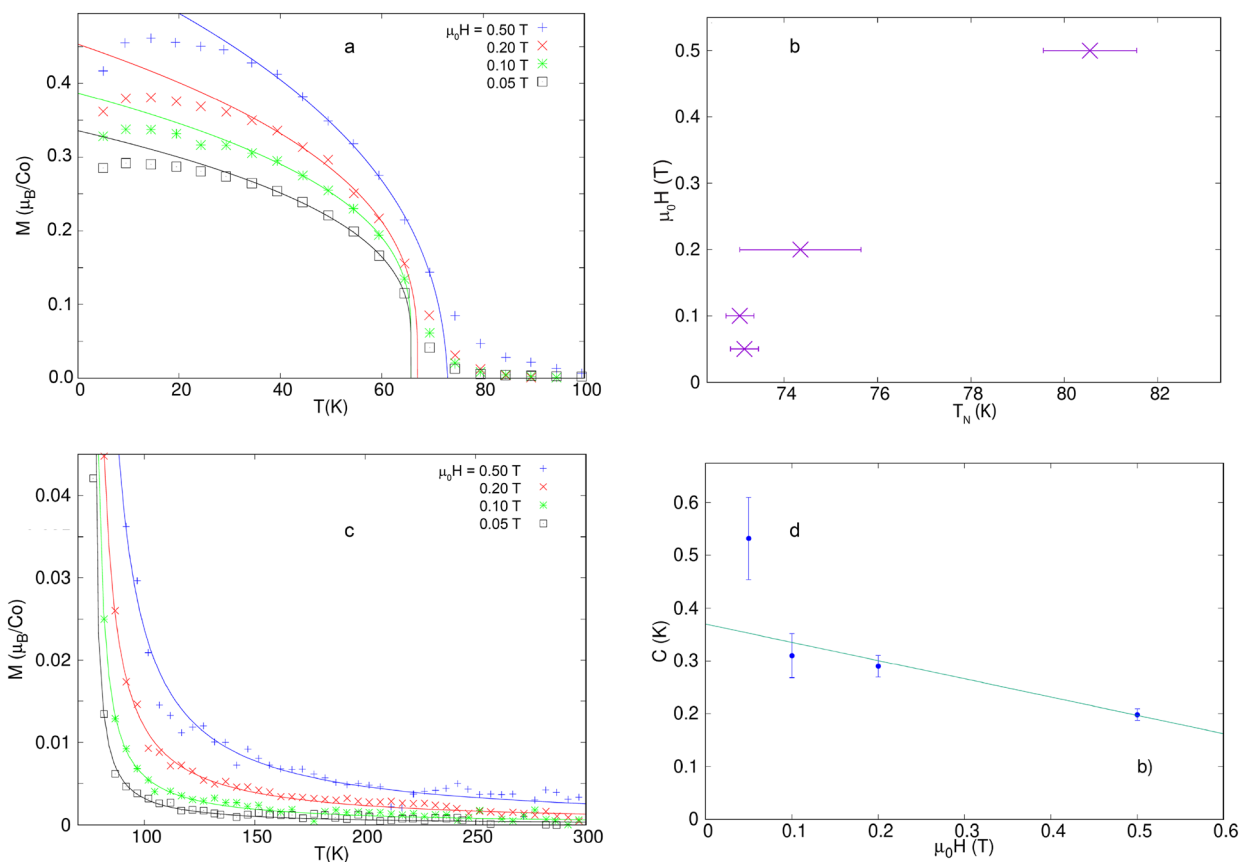
from the induced spin-flop moment that normally occurs even with collinear sublattices. The spin-flop component is expected to decrease at low T as the antiferromagnetic susceptibility decreases to zero. The fitted values of $T_N(H)$ are plotted versus H in Fig. 8(b) and the result is typical of a phase diagram near a bicritical or tetracritical point. Significantly, above a small value of H, T_N increases with H, which is typical behavior expected for a nearly Heisenberg antiferromagnetic material just above the bicritical or tricritical point; such behavior would not be expected for either a ferromagnetic or an antiferromagnetic material with strongly anisotropic exchange interactions. The decrease in M at low temperatures and the increase of $T_N(H)$ with field strongly indicate that the system is a fairly isotropic exchange antiferromagnet with non-collinear sublattice magnetizations. The relatively weak anisotropy indicated by $T_N(H)$ in Fig. 8(b) is not compatible with a description of the large anisotropy indicated by M vs. T for fields in the plane parallel to the substrate interface and perpendicular to it shown in Fig. 4. The anisotropy exhibited in that figure is, however, consistent with non-collinear antiferromagnetic sublattices with components of the moments in the plane parallel to the interface interacting with a nearly isotropic exchange interaction.

The field-dependent behavior above T_N is shown in Fig. 8(c). The curves are fits to Curie–Weiss behavior. Normally, for small applied fields, the constant C is independent of the applied field H, which means that the magnetization M is proportional to H. However, this is not the case, as shown in Fig. 8(d). Corrections to the Curie–Weiss behavior at larger fields should go as $(M/M_0)^2$, where M_0 is the maximum moment. The value of M_0 can be taken as the value of approximately $3\mu_B$ from the fits at $\mu_0 H = 0.1$ T (Table 2). Comparing this to the values of M in Fig. 8(c), it is clear that corrections to Curie–Weiss cannot explain the non-linearity in Fig. 8(d). However, the component of the moment in the plane of the substrate interface is partly a result of the distorted oxygen octahedral environment at each Co site, as discussed below. The size of the field-induced moment is influenced by the degree of canting of the moments caused by the non-cubic environment at each Co site and that geometric effect does not grow in proportion to the applied field.

The correlation between the Co–O–Co bond angle and the magnetization

Insight into the behavior of the LCO films can be gained by making comparisons to bulk LCO, where antiferromagnetic interactions are highly correlated with the Co–O–Co angle and are suppressed for angles below $163°$. The experimental observations are consistent with calculations predicting the critical angle necessary for magnetic interactions [6]. Although that correlation has not been calculated for the film environment where LCO is distorted by sublattice strain, from the observed behavior

Figure 7: Magnetization M as a function of the external field $\mu_0 H$ for a 26.0-nm LCO film grown on a LAO substrate showing a small hysteresis and that of a 25.7-nm film grown on a STO substrate with a larger hysteresis (coercivity) plotted together for comparison.

Figure 8: (a) Fits using Eq. 2 with $\beta = 0.37$ (solid curves) to the critical behavior of the magnetization M vs. temperature T data below the transition measured at different external fields $\mu_0 H$ (see legend) for the 25.7-nm LCO sample on STO. (b) The increase in $T_N(H)$, determined from the fits in (a), with the application of relatively small fields is typical behavior of an antiferromagnetic material with nearly isotropic exchange interactions. The point of minimum T_N near $\mu_0 H = 0.15\,T$ can be bicritical or tetracritical, depending on the sign of the cubic anisotropy [32]. (c) Magnetization M vs. temperature T for $T > T_N$ with fits to Curie–Weiss behavior over the temperature range $82 < T < 300$ K measured at different external fields $\mu_0 H$ (see legend) for the 25.7-nm LCO sample on STO. (d) The Curie–Weiss parameter C as a function of the external field H showing unusual nonlinear behavior despite the small-induced magnetization region. The green line is a linear fit to the data.

in films discussed below it appears that the general magnetic behavior approximately conforms to the same dependence of the magnetic interactions on the Co–O–Co angle.

Although the lattice parameters of the films have been measured only at room temperature, we can estimate the structure at low temperature assuming similar relative changes in the a and c pseudocubic lattice parameters upon cooling as observed in bulk LCO. LCO parameters shorten by approximately 1% (as do the parameters in LAO and STO [33, 34]). The Co–O bond length in LCO shortens by approximately 0.5% upon cooling from room temperature to low temperature. The most relevant effect of cooling from room temperature in bulk LCO is to reduce the Co–O–Co angle by about one degree, which is important because the bulk Co–O–Co angle at room temperature is near the critical value of 163° and it decreases to that critical value near $T = 40$ K.

Neutron and x-ray scattering and EXAFS spectroscopy techniques have been used to study the details of the temperature

dependence of the lattice parameters in bulk LCO [3, 9]. EXAFS data were also used to determine the Co–O bond length in LCO films on LAO and STO substrates [22] along directions parallel and perpendicular to the substrate interface. When possible, lattice parameters are most accurately determined using scattering techniques, but the amount of material in thin films makes an accurate determination of the Co–O bond length difficult. However, EXAFS spectroscopy has been used to accurately determine the ratio of the Co–O bond lengths that are approximately along the c-axis and a-axis. For LCO on LAO, the ratio of the Co–O bond length along the c-axis to that along a-axis is determined to be 1.003(4), which is close to unity, and the ratio for LCO on STO is 0.979(6), which significantly deviates from unity. Because the LCO films have the same chemical environment as bulk LCO, we assume in our discussion that the Co–O bond lengths in the films are only altered when necessary to conform to the lattice mismatch between the film and substrate.

We assume that the Co–O bond lengths for LCO films on LAO are close to the bulk LCO value of 1.924(2) Å at room temperature and 1.915(2) Å at low temperature obtained from other studies [2, 4, 8]. However, the average measured c lattice parameters for the film, listed in Table 1, is 3.87 Å, which is slightly larger than twice the room-temperature bulk Co–O bond length of 3.85 Å. Note, however, that in bulk LCO, the c lattice parameter decreases slightly more than the Co–O bond length as the temperature decreases, so the film c parameter and the Co–O bond length possibly agree even better at low temperatures. For the c lattice parameter to be twice the bulk Co–O bond length, or perhaps slightly stretched to fit the Co–Co bond length, suggests that the Co–O bond is close to being aligned with the c-direction and the Co–O–Co bond angle is close to 180°. If Co–O bond length is actually one or two percent larger than the c parameter, the Co–O–Co angle will not be significantly smaller than 180°; it will not be close to the critical angle of 163°. Assuming the other two Co–O bonds are perpendicular to this one, they must lie nearly in the plane parallel to the substrate interface. To accommodate the room-temperature lattice parameter $a = 3.791$ Å, the Co–O–Co bond angles must be close to 160° and we would expect this angle to decrease upon cooling as it does in bulk LCO. In bulk LCO, Co–O–Co angles less than 163° prevent magnetic interactions [3]. If we assume a similar cut-off angle in the LCO films on LAO substrates, we would expect the interactions between Co sites along the direction perpendicular to the substrate interface to be strong, but there should be no significant magnetic interaction in the plane parallel to the interface. This magnetic interaction geometry would support a one-dimensional magnetic system, but one-dimensional magnets cannot exhibit long-range order. This is consistent with the observation from magnetometry experiments that, in the thinnest films, no phase transition to long-range order takes place. To form a Co–O–Co angle greater than 163° to support antiferromagnetic interactions, the Co–O bonds parallel to the substrate interface would need to be 1.917 Å or smaller at room temperature. There is no reason for Co–O bond to shorten from the room-temperature bulk value, however, because that is not required to accommodate the substrate lattice parameter.

In the thicker LCO films on LAO substrates, a spin-flop-like transition is observed and the moment at low temperature grows with increasing thickness. The thicker films also exhibit a new peak in the Bragg scattering as shown in Fig. 2 that suggests a relaxation of the lattice toward bulk LCO lattice parameters. Table 1 shows that the secondary peak corresponds to a vertical c-axis lattice parameter of 3.818 Å, close to the bulk value. Interestingly, the change in the lattice structure appears abrupt rather than continuous. AFM images (Fig. S6, Supplementary Material) show the surface of the film acquiring a granular texture and this is likely that results from relaxed non-epitaxial material with an altered structure, similar to the NbO_2 epitaxial

films discussed elsewhere [35]. Once the lattice parameters allow for Co–O–Co angles larger than about 163° in all directions, three-dimensional magnetic ordering is possible. The behaviors of the thin and thick films prove consistent with the geometric model for the correlation of the magnetic behavior with the Co–O–Co critical angle in bulk and nanoparticle LCO.

LCO films on STO substrates represent a quite different strain configuration. Instead of compressing the Co–O bonds along the a-axis, they are significantly stretched. The room-temperature a-axis lattice parameter is 3.905 Å, significantly larger than 3.85 Å, twice the bulk LCO Co–O bond length of 1.924(2) Å. Transmission electron microscopy (TEM) measurements [14] confirm that the Co–O–Co angle is close to 180° in that plane and that condition is likely unchanged upon cooling. It is unlikely that the Co–O bond could be even larger than required to fit along the a-axis of the lattice. If the third Co–O bond is perpendicular to the other Co–O bonds, it must be significantly compressed relative to the others and to the bulk Co–O bond length. The c-axis lattice parameter for 22.3-nm and 25.7-nm thick films on STO is 3.79 Å, which is significantly smaller than twice the bulk LCO Co–O bond length, 3.85 Å, by a ratio of 0.984. XAFS measurements [22] indicate the ratio of the Co–O bond length along the c-axis to that along a-axis is 0.979(6), which is consistent with the compression of the Co–O bond needed to fit the c-axis lattice parameter and suggests that the Co–O bond is nearly aligned with the c-axis. Upon cooling, the lattice structure might change slightly, but clearly all of the Co–O–Co angles are much larger than 163° if all the Co–O bonds are nearly perpendicular to each other.

The thinner films on STO substrates, 10.3 and 7.8 nm, show slightly larger compression in the c-axis direction, with a ratio of the c-axis to the a-axis lattice parameters equal to 0.96, than 22.3- and 25.7-nm films, but the net moments at low temperature are comparable; all four samples show a net moment between 0.30 and 0.44 μ_B. In Fig. 2(c), a small peak is evident just below 76° for 22.3-nm film, approximately at the angles of the film peaks of thinner (10.3 and 7.8 nm) films. This might represent the layers adjacent to the substrate of the thicker film that have not relaxed as much.

Unequal Co–O bonds along the a-axis and c-axis directions should result in the loss of cubic symmetry experienced by the magnetic moments centered on the Co sites. It is also possible that the perpendicular Co–O bonds are not exactly along the c-axis to avoid some of the compression. That would also result in the loss of cubic symmetry. In either case, with the loss of cubic symmetry, the magnetic moments associated with each Co site could misalign with the c-axis and, with antiferromagnetic ordering, the tilt direction would then alternate from layer to layer. Twin domains with 90° rotations would also be expected with a tilt and twinning has been observed [13]. The resulting non-collinear alignment of the moments would result in a net

moment perpendicular to the c-axis, a condition consistent with the observation from magnetometry experiments that the net moment is predominantly, if not entirely, in the plane of the interface. It is likely that the origin of the net moment in an LCO film on a STO substrate is the canting of the antiferromagnetic sublattices. If the magnetic sublattices create a net moment, we can estimate the angle of tilt from the c-axis by comparing net moment achieved at low T with the moment on each Co site. The net moment per Co site is 0.44 μ_B, whereas the moment on each Co, from Table 2, is approximately 3.3 μ_B, which corresponds to a tilt angle as large as 8°, assuming moments at all Co sites contribute to the long-range order.

An early attempt [7] to address the magnetic behavior of bulk LCO invoked a distortion of the oxygen octahedra as a mechanism for generating magnetic moments on the Co sites above $T = 40$ K. However, it was shown [8, 9] that any distortion is too small to account for the moment. On the other hand, the Co–O–Co angle was shown [2, 3, 6] to be strongly correlated with the appearance of the moment in both experiments and extended state theory. For the STO substrate, the EXAFS measurements indicate a small bond difference of 2%. Although we show in the present work that the Co–O–Co angles alone are sufficient to explain the observed magnetic behavior, one could consider if some generalization of the local state picture could play a significant role as well since there is a small octahedral distortion. However, the measured moments in the bulk and film are quite similar, so the distortion must, at most, play a minor role in producing the observed moment per Co site in the film. Also, the large anisotropy of the observed moment in the film is not easily explained in the context of local moments on the Co sites that interact ferromagnetically; the moments would need to be dominated by a large planar anisotropy. The highly anisotropic net moment is, on the other hand, entirely consistent with moments that cant by a relatively small angle ($< 10°$) away from the axis perpendicular to the substrate interface as a result of the loss of cubic anisotropy of the slightly distorted oxygen octahedra surrounding the Co ions.

Cubic anisotropy in a nearly isotropic exchange antiferromagnet can result in antiferromagnetic state if it favors spins aligning along the axes of the cubic anisotropy, in our case along the diagonals of the oxygen octahedra. It can cause a biconical state when it favors spins aligning away from the axes and this would result in a net moment along the field [1]. One might expect that the latter case fits the LCO on a STO substrate case which exhibits a net moment. However, a thick LCO film on a LAO substrate has no net moment, indicating that the cubic anisotropy favors alignment along the axes when the oxygen octahedra are not distorted. The distortion of the octahedra in LCO on STO could result in a biconical state if the spins cannot align with the octahedral axes. A ground state calculation

similar to that of an undistorted cubic anisotropy has not been done, to the best of our knowledge.

A resonant x-ray scattering study [15] of a LCO film on a STO substrate was interpreted to suggest charge ordering at and below room temperature, where adjacent Co sites are in alternating low-spin (LS) and high-spin (HS) states, and the magnetic interactions are ferromagnetic and exist only between second-nearest HS neighbors. The experimental data were interpreted in the context of a DFT calculation where such a spin-state ordering is imposed. Although the calculations and resonant scattering results are internally consistent, the *a priori* imposition of spin-state ordering does not necessarily exclude a model where the interactions are antiferromagnetic and similar to bulk LCO, but are associated with distorted oxygen octahedra. It would be useful to compare density functional theory (DFT) calculations under these conditions with the resonant x-ray scattering data [15].

Conclusion

We have demonstrated that the magnetic behavior of LaCoO$_3$ on both LaAlO$_3$ and SrTiO$_3$ substrates is consistent with nearly isotropic antiferromagnetic exchange interactions and significant cubic anisotropy associated with the oxygen octahedra surrounding each Co site. In the case of STO on LAO substrates, the ordering is suppressed close to the substrate interface and that correlates well with the Co–O–Co angle. We have also shown how the appearance of a net moment in LCO films on STO substrates is a result of non-collinear antiferromagnetic sublattices and again correlates well with the Co–O–Co bond angle. That correlation provides insight into why LCO films can exhibit a net moment or not depending on the strain from the substrate. It also demonstrates that a detailed understanding of the magnetic interactions in bulk LCO is key to understanding them in thin films. In our experiments, LCO films grown on LAO substrates where LAO provided a compressive strain to the film ($a/c < 1$) have no magnetic ordering for strained films near the substrate interface and spin-flop-like (canted) ordering in partially relaxed thicker films. The films grown on STO substrates with biaxial tensile strain ($a/c > 1$), on the other hand, showed an abrupt increase in moment below 80 K. M vs. T measurements in the films grown on STO follow critical behavior with a critical exponent consistent with the Heisenberg 3D value ($\beta = 0.37$). Together with the decrease of M as $T \to 0$ and an increasing T_N with field, we conclude that this system has a weak magnetic anisotropy and a non-collinear sublattice magnetization. The effective moment per Co ion ($\mu_{\text{eff}} \gtrsim 3\mu_B$), on the other hand, remains consistent with that of bulk LCO.

It has been demonstrated that substrate strain can be used to switch between states with and without net moments in a

LCO/STO film, for example, by applying voltages to the SrTiO$_3$ film; this forms the basis of a low-temperature logic device [10]. As discussed above, with no voltage applied to the STO substrate, the octahedra surrounding the Co ions are distorted, resulting in non-collinear alignment of the antiferromagnetic moments. The geometric mechanism for the switching is that a voltage applied to the STO substrate decreases the LCO lattice parameters in the interface plane, thereby allowing the lattice parameter perpendicular to the plane to increase. This allows the LCO octahedra to relax into a non-distorted shape and the antiferromagnetic moments become collinear. Although LCO can be used to create logic devices, the magnetic system only orders below approximately 90 K. A more practical device would require a switchable net magnetic moment above room temperature. To achieve switching in the antiferromagnetic film layer, two mechanisms are possible based on the geometric influences on the magnetic moment observed in LCO. First, if a material with an octahedral twist close enough to the critical angle could be stressed, the magnetism could be turned on and off with stress from a piezoelectric or ferroelectric substrate, such as STO. Second, if the lattice of the film is distorted by the constraints imposed by the substrate, an antiferromagnetic system could be switched from non-collinear to collinear order. The latter mechanism might be the easier one to realize. The consideration of the geometric effects and strain on thin antiferromagnetic films opens up new avenues for discovering appropriate magnetic thin film and substrate combinations that can lead to the development of new, practical electronic logic devices at higher temperatures than that of the LCO/STO device. From a device production point of view, an important issue to resolve is the need to obtain epitaxial growth, which requires precise temperature and oxygen pressure control, as well as growth on crystals like LAO or LCO instead of more widely available substrates used in industry like silicon.

Methodology

Sample growth

Before growth, single-crystalline SrTiO$_3$ (STO) (001) and LaAlO$_3$ (LAO) (001) substrates were cleaned by sonicating in acetone and isopropanol for 10 min each. In addition, STO substrates were annealed twice at 1000 $^\circ$C for 2 hrs in an atmospheric annealing furnace (Lindberg/Blue M), followed by a 30-s deionized water etch as discussed in Ref. [36]. The procedure results in a TiO$_2$-terminated atomically flat surface with a step-terrace structure.

All films were grown using a pulsed laser deposition (PLD) technique. A stoichiometric LaCoO$_3$ target was ablated using a 248-nm wavelength KrF excimer laser (Coherent Compex Pro F 102). Samples were mounted to the substrate holder using high-vacuum compatible conductive silver paint (Ted Pella, Inc.) to maximize thermal contact with the substrate heater. During growth, the substrate temperature was kept at 650 $^\circ$C, and the chamber pressure was maintained at 200 mTorr with 120-sccm constant flow of ultrahigh purity O$_2$ gas. After growth, the sample temperature was decreased to room temperature at a rate of 20 $^\circ$C/min in an ambient growth pressure.

Structural characterization

Crystal quality was monitored during sample growth using *in situ* reflection high-energy electron diffraction (RHEED) and sample topography was measured after growth using tapping mode atomic force microscopy (AFM) at room temperature (Oxford Cypher AFM). Epitaxial strain on the films was quantified using x-ray diffraction spectra measured using a Rigaku Smartlab using Cu K$_{\alpha_1}$ radiation. Thin films lattice parameters were calculated using Bragg peaks fitted to a Gaussian function and the film thickness was estimated using low-angle x-ray reflectivity data analyzed using GenX software [37]. In addition, x-ray scattering data were obtained at 10 keV energy at BL14B1 of the Shanghai Synchrotron Radiation Facility (SSRF) [38]. Two LCO films grown on LAO substrates and two films grown on STO substrates were measured using a Huber 5021 six-circle diffractometer [39].

Measurement of magnetic properties

Magnetometry data were taken using a superconducting quantum interference device (SQUID) magnetometer (Quantum Design MPMS XL) with the reciprocating sample option (RSO) method of measurement. Each sample was measured with the field oriented in the plane as well and out of the plane. Samples were cooled in a $\mu_0 H = 100$ mT field from $T = 320$ K to 5 K at a rate of 5 K/min and the magnetization was measured at a temperature interval of 1 K while cooling the sample at a rate of 2 K/min. To eliminate the diamagnetic contribution from the substrates, after measuring a sample, the film was etched off the substrate by chemically dipping the sample into aqua regia for 30 s. The magnetic measurements were then repeated on the substrate with both field orientations with identical measurement conditions. After proper subtraction of the signal from the substrate, the data were fitted to the Curie–Weiss model with an additional constant background term.

Acknowledgments

Data availability

All data that support the findings of this study are included within the article and supplementary files.

Code availability

Not applicable.

Declarations

Conflict of interest The authors declare no conflicts of interest nor competing interests.

Supplementary Information

The online version contains supplementary material available at https://doi.org/10.1557/s43578-023-00957-3.

References

1. G.M. Kaminsky, D.P. Belanger, F. Ye, J.A. Fernandez-Baca, J. Wang, M. Matsuda, J.-Q. Yan, Phys. Rev. B **97**, 024418 (2018)

2. A.M. Durand, D.P. Belanger, C.H. Booth, F. Ye, S. Chi, J.A. Fernandez-Baca, M. Bhat, J. Phys.: Condens. Matter **25**, 382203 (2013)

3. D.P. Belanger, T. Keiber, F. Bridges, A.M. Durand, A. Mehta, H. Zheng, J.F. Mitchell, V. Borzenets, J. Phys.: Condens. Matter **28**, 025602 (2016)

4. A.M. Durand, D.P. Belanger, T.J. Hamil, F. Ye, S. Chi, J.A. Fernandez-Baca, C.H. Booth, Y. Abdollahian, M. Bhat, J. Phys.: Condens. Matter **27**, 176003 (2015)

5. A.M. Durand, T.J. Hamil, D.P. Belanger, S. Chi, F. Ye, J.A. Fernandez-Baca, Y. Abdollahian, C.H. Booth, J. Phys.: Condens. Matter **27**, 126001 (2015)

6. Y. Lee, B.N. Harmon, J. Appl. Phys. **113**, 17E145 (2013)

7. M.A. Korotin, S.Y. Ezhov, I.V. Solovyev, V.I. Anisimov, D.I. Khomskii, G.A. Sawatzky, Phys. Rev. B **54**, 5309 (1996)

8. N. Sundaram, Y. Jiang, I.E. Anderson, D.P. Belanger, C.H. Booth, F. Bridges, J.F. Mitchell, T. Proffen, H. Zheng, Phys. Rev. Lett. **102**, 026401 (2009)

9. Y. Jiang, F. Bridges, N. Sundaram, D.P. Belanger, I.E. Anderson, J.F. Mitchell, H. Zheng, Phys. Rev. B **80**, 144423 (2009)

10. C.Q. Hu, K.W. Park, A. Posadas, J.L. Jordan-Sweet, A.A. Demkov, E.T. Yu, J. Appl. Phys. **114**, 183909 (2013)

11. G. Zhou, X. Wang, H. Ji, J. Zhang, P. Kang, Z. Li, J. Magn. Magn. Mater. **515**, 167303 (2020)

12. Q. Feng, D. Meng, H. Zhou, G. Liang, Z. Cui, H. Huang, J. Wang, J. Guo, C. Ma, Z. Zhai, Q. Lu, Y. Lu, Phys. Rev. Mater. **3**, 074406 (2019)

13. E.-J. Guo, R.D. Desautels, D. Keavney, A. Herklotz, T.Z. Ward, M.R. Fitzsimmons, H.H. Lee, Phys. Rev. Mater. **3**, 014407 (2019)

14. S. Li, J. Wang, Q. Zhang, M.A. Roldan, L. Shan, Q. Jin, S. Chen, Z. Wu, C. Wang, C. Ge, M. He, H. Guo, L. Gu, K.J. Jin, E.-J. Guo, Phys. Rev. Mater. **3**, 114409 (2019)

15. G. Sterbinsky, R. Nanguneri, J.X. Ma, J. Shi, E. Karapetrova, J. Woicik, H. Park, J.-W. Kim, P. Ryan, Phys. Rev. Lett. **120**, 197201 (2018)

16. H. Zhang, J. Zhang, H. Yang, Q. Lan, D. Hong, S. Wang, X. Shen, T. Khan, R. Yu, J. Sun, B. Shen, Appl. Mater. Interfaces **8**, 18328 (2016)

17. V.V. Mehta, N. Biskup, C. Jenkins, E. Arenholz, M. Varela, Y. Suzuki, Phys. Rev. B **91**, 144418 (2015)

18. L. Qiao, J.-H. Jang, D.-J. Singh, Z. Gai, H. Xiao, A. Mehta, R.-K. Vasudevan, A. Tselev, Z. Feng, H. Zhou, S. Li, W. Prellier, X. Zhu, Z. Liu, A. Borisevich, A.-P. Baddorf, and M.-D. Biegalski, Nano Lett. , 4677 (2015)

19. J. Fujioka, Y. Yamasaki, A. Doi, H. Nakao, R. Kumai, Y. Murakami, M. Nakamura, M. Kawasaki, T. Arima, Y. Tokura, Phys. Rev. B **92**, 195115 (2015)

20. J.-H. Kwon, W.S. Choi, R.J.Y.-K. Kwon, J.-M. Zuo, H.N. Lee, M. Kim, Chem. Mater. **26**, 2496 (2014)

21. W.S. Choi, J.H. Kwon, H. Jeen, J.E. Hamann-Borrero, A. Radi, S. Macke, R. Sutarto, F. He, G.A. Sawatzky, V. Hinkov, M. Kim, H.N. Lee, Nano Lett. **12**, 4966 (2012)

22. G.E. Sterbinsky, P.J. Ryan, J.-W. Kim, E. Karapetrova, J.X. Ma, J. Shi, J.C. Woicik, Phys. Rev. B **85**, 020403 (2012)

23. A.D. Rata, A. Herklotz, L. Schultz, K. Dorr, Eur. Phys. J. B **76**, 215 (2010)

24. V.V. Mehta, M. Liberati, F.J. Wong, R.V. Chopdekar, E. Arenholz, Y. Suzuki, J. Appl. Phys. **105**, 07E503 (2009)

25. D. Fuchs, E. Arac, C. Pinta, S. Schuppler, R. Schneider, H.V. Lohneysen, Phys. Rev. B **77**, 014434 (2008)

26. A. Herklotz, A.D. Rata, L. Schultz, K. Dorr, Phys. Rev. B **79**, 092409 (2009)

27. S. Park, P. Ryan, E. Karapetrova, J.W. Kim, J.X. Ma, J. Shi, J.W. Freeland, W. Wu, Appl. Phys. Lett. **95**, 072508 (2009)

28. J.W. Freeland, J.X. Ma, J. Shi, Appl. Phys. Lett. **93**, 212501 (2008)

29. E.-J. Guo, R. Desautels, D. Keavney, M.-A. Roldan, B.-J. Kirby, D. Lee, Z. Liao, T. Charlton, A. Herklotz, T.-Z. Ward, M.-R. Fitzsimmons, H.-N. Lee, Sci. Adv. **5**, eaav5050 (2019). https://doi.org/10.1126/sciadv.aav5050

30. K. Binder, P.C. Hohenberg, Phys. Rev. B **6**, 3461 (1972)

31. K. Binder, P.C. Hohenberg, Phys. Rev. B **9**, 2195 (1974)

32. E. Domany, M.E. Fisher, Phys. Rev. B **15**, 3510 (1977)

33. R. Loetzsch, A. Lübcke, I. Uschmann, E. Förster, V. Große, M. Thuerk, T. Koettig, F. Schmidl, P. Seidel, Appl. Phys. Lett. **96**, 071901 (2010). https://doi.org/10.1063/1.3324695

34. S.-A. Hayward, F.-D. Morrison, S.-A.-T. Redfern, E.-K.-H. Salje, J.-F. Scott, K.-S. Knight, S. Tarantino, A.-M. Glazer, V. Shuvaeva, P. Daniel, M. Zhang, M.-A. Carpenter, Phys. Rev. B **72**, 054110 (2005). https://doi.org/10.1103/PhysRevB.72.054110

35. T. Joshi, E. Cirino, S.-A. Morley, D. Lederman, Phys. Rev. Mater. **3**, 124602 (2019). https://doi.org/10.1103/PhysRevMaterials.3.124602

36. J.G. Connell, B.J. Isaac, G.B. Ekanayake, D.R. Strachan, S.S.A. Seo, Appl. Phys. Lett. **101**, 251607 (2012). https://doi.org/10.1063/1.4773052

37. M. Björck, G. Andersson, J. Appl. Crystallogr. **40**, 1174 (2007). https://doi.org/10.1107/S0021889807045086

38. W. Yang, T.-Y. Wen, G.-Z. Yin, X.-L. Li, M. Gao, Y.-L. Gu, L. Li, Y. Lu, H. Lin, X.-M. Zhang, B. Zhao, T.-K. Lin, Y.-G. Yang, Z. Li, X.-T. Zhou, X.-Y. Gao, Nucl. Sci. Technol. **26**, 020101 (2016). https://doi.org/10.13538/j.1001-8042/nst.26.020101

39. M. Gao, Y. Gu, L. Li, Z. Gong, X. Gao, W. Wen, J. Appl. Crystallogr. **49**, 1182 (2016). https://doi.org/10.1107/S1600576716008566